

Crystallization process of a three-dimensional complex plasma

Benjamin Steinmüller,^{*} Christopher Dietz, Michael Kretschmer, and Markus H. Thoma

Institute of Experimental Physics I, Justus Liebig University Giessen, Heinrich-Buff-Ring 16, 35392 Giessen, Germany



(Received 24 October 2017; revised manuscript received 5 December 2017; published 7 May 2018)

Characteristic timescales and length scales for phase transitions of real materials are in ranges where a direct visualization is unfeasible. Therefore, model systems can be useful. Here, the crystallization process of a three-dimensional complex plasma under gravity conditions is considered where the system ranges up to a large extent into the bulk plasma. Time-resolved measurements exhibit the process down to a single-particle level. Primary clusters, consisting of particles in the solid state, grow vertically and, secondarily, horizontally. The box-counting method shows a fractal dimension of $d_f \approx 2.72$ for the clusters. This value gives a hint that the formation process is a combination of local epitaxial and diffusion-limited growth. The particle density and the interparticle distance to the nearest neighbor remain constant within the clusters during crystallization. All results are in good agreement with former observations of a single-particle layer.

DOI: [10.1103/PhysRevE.97.053202](https://doi.org/10.1103/PhysRevE.97.053202)

I. INTRODUCTION

The crystallization process of various materials are of great interest in solid state physics. In actual materials, the specific timescales and size scales make a detailed study of the involved processes unattainable. Computer simulations [1] or model systems such as colloidal systems [2] and complex plasmas [3] may help to overcome these limitations. In complex plasmas the length scales and timescales are in the range of minutes and millimeters. The positions of each individual particle, as well as collective effects in the aggregation process, can be recorded [4]. The timescales in colloidal systems range from seconds to days and the length scales are in the range of the wavelength of visible light [5].

A complex plasma consists of micron-sized particles embedded in a low-temperature plasma. These particles charge up negatively due to the high electron velocity and interact via the Yukawa potential. Depending on the ratio of the interacting energy to the thermal energy, the particles may arrange in solid or liquid configurations [3]. Under laboratory conditions, the particles have to be levitated to counter gravity, e.g., by an electric field. Owing to the screening of electric fields in the plasma, the particles are often arranged in a single layer or in a few layers located in the sheath [6]. Since all particles can be observed simultaneously in a single layer, the melting [7–9] and crystallization [10] of flat complex plasmas are well understood. Under certain conditions (small particles and a strong confinement), it is possible that the particle cloud ranges up into the presheath and bulk plasma even in ground-based experiments [11,12]. Also, computer simulations were performed to study the phase transition of three-dimensional complex plasmas [13,14].

A widespread method to analyze the process of aggregation in detail is the determination of the fractal dimension [15–17]. In epitaxial growth (at least at the beginning), one layer after

another settles on the surface, creating compact objects with the same dimension as of the embedding Euclidean space [18]. A different picture is shown by diffusion-limited growth, where the exposed ends of a structure screen their own center. As a result, the ends grow faster than the remaining parts and branched complex objects are created [19,20]. In three-dimensional embedding Euclidean space, the fractal dimension for irreversible diffusion-limited cluster-cluster aggregation (DLCA) [21] is $d_f = 1.78 \pm 0.06$, and for irreversible diffusion-limited aggregation (DLA) [22] it is $d_f = 2.53 \pm 0.06$ [19]. If the growth is reversible, the bonds can be destroyed and the particles can rearrange, creating much more compact objects. For this reason, reversibility increases the fractal dimension of the grown structures towards the value for the embedding Euclidean dimension [17].

Rubin-Zuzici *et al.* [13] have examined a contour in a two-dimensional slice of a three-dimensional complex plasma during the phase transition. It is shown that the fractal dimension d'_f of the crystallization front line oscillates between 1.16 and 1.21. This is higher than for epitaxially grown structures (in this context, $d = 1$) and lower for diffusion-limited growth (in this context, $d_f = 1.42$) [13]. For a two-dimensional slice, the overall fractal dimension of the crystallization front is decreased by 1 [23]. This means that in the originally embedding three-dimensional Euclidean space, the front area has a fractal dimension of $d_f = 2.16$ – 2.21 .

Previously, only colloidal systems were used as model systems to observe the aggregation process in three dimensions. Based on the high fluid density of the surrounding fluid, the colloidal systems are overdamped. Due to the low damping rate, complex plasmas may provide new insights into the phase transition process in general [24].

In the presented work, the crystallization process of a liquidlike three-dimensional complex plasma under gravity conditions is studied. The measurements are time and space resolved. A local criterion shows individual particles in the solid state at particular time steps, from which the fractal dimension of the clusters can be derived.

^{*}Benjamin.Steinmueller@physik.uni-giessen.de

II. EXPERIMENTAL SETUP AND PROCEDURE

A capacitively coupled radio-frequency chamber with a frequency of 13.56 MHz (peak-to-peak voltage of 15 V at the lower and 35 V at the upper electrode) is used for the experiments. The electrodes have a diameter of 7.5 cm and are 3 cm apart from each other, and the diameter of the chamber is 14 cm. Glass coated with indium tin oxide (ITO) is used as the upper electrode. Due to the transparency of this electrode, it is possible to mount the camera directly above it. The melamine-formaldehyde particles inside the complex plasma have a diameter of $d = 2.05 \pm 0.04 \mu\text{m}$ and are injected by a dispenser mounted on the side of the chamber. Due to the small particle mass, a weak electric field in the bulk plasma is sufficient for levitation. Besides the electric field and the gravity, no significant forces act on the particle. A guard ring around the lower electrode is responsible for the horizontal confinement of the particle cloud. The experiments described here are performed in argon at a pressure of 40 Pa. To illuminate the particles, a laser beam (width ≈ 0.1 mm) is spread into a sheet parallel to the electrodes. The laser light, which is scattered by the particles, is recorded by a camera perpendicular to the laser sheet. Further information about the experimental setup is given in Ref. [11].

To observe its phase transition from a liquid- to crystal-like system, the complex plasma has to be fully disordered in the beginning. This is achieved by a temporal increase of rf power to a peak-to-peak voltage of 52 V at the lower and 92 V at the upper electrode, in which the particles gain a high kinetic energy [9]. When the power is reduced again, crystallization starts. Three-dimensional positions of the particles are acquired by moving the laser diode, as well as the camera, in a vertical direction perpendicular to the electrodes. Several scans are taken at different times, in order to get time-resolved measurements. A scan with a speed of 0.1 mm/s starts at the upper part of the complex plasma and ends in the lower part [25]. The next scan goes from the lower to the upper part, with each scan taking about 33 s. This scan velocity is of the same order as used in other plasma crystal experiments [12,26–29]. To reconstruct the position of the particles, first, the particles are identified in each single frame with subpixel accuracy and then they are tracked over consecutive frames [30]. The z coordinate of the particles is calculated by the position of the laser sheet above the electrode. Particles in the solid state oscillate around their equilibrium positions [31], with an amplitude of about 23 μm in the x and y directions. Due to the low scanning speed, with this method it is possible to gain the exact equilibrium positions of the particles in the horizontal plane by averaging over time since the particles are identified in several frames. Due to the fact that this is not possible for the scan direction, the z coordinate has an uncertainty in the range of the oscillation amplitude. Assuming a typical thermal energy (~ 0.025 eV), particles in the liquid state have a higher kinetic velocity than the scanning speed. This is a widespread issue in three-dimensional complex plasmas [12,26–29] or even in two dimensions, where a particle can move between two frames further than the mean interparticle distance [13]. As a result, only the positions of particles in the solid state are determined with high accuracy, while the positions of particles in the liquid state have large uncertainties.

The drawback of the scanning method is that not all particles are recorded simultaneously. The scans are done 0, 33, 66, 99, 178, 211, and 244 s after reducing the rf power. In the following, the particle positions are named after the starting time of the corresponding scan. The complementary metal-oxide semiconductor (CMOS) camera has a resolution of 15.6 $\mu\text{m}/\text{pixel}$ and a frame rate of 40 fps. The region of interest of about $10 \times 10 \times 4 \text{ mm}^3$ contains over 36000 particles. The examined region is chosen from the homogeneous center of the particle cloud, 3.5 mm above the lower electrode, which is above the sheath region with a maximal extension of about 1 mm [32] (Debye length $\sim 100 \mu\text{m}$). Taking an even distribution of particles within the confinement into account, the whole cloud consists of about 1.6×10^6 particles. Since no gas flux is present, the particles do not move collectively, nevertheless, some particles can diffuse inside and outside of the examined region.

III. FRACTAL SCALE ANALYSIS

In a complex plasma, three different crystalline structures can occur: hexagonal closed packed (hcp), face-centered cubic (fcc), and body-centered cubic (bcc). In this investigation, the exact crystal structure is not important, but a reliable identification of whether a single particle is in the liquid or in the solid state is important. This is why the scalar product of the Minkowski structure metric (SPMSM) is applied. This method is robust against uncertainties up to 14% of the nearest-neighbor distance in the particle positions, e.g., because of oscillation in the scan direction. This is why the x and y coordinates of the particles have to be determined with high accuracy, otherwise the sum of the errors in each direction would be too high for a reliable identification via the SPMSM [11,33–35].

For a particle i , the order parameters

$$q_{6m}(i) = \sum_{f \in \mathcal{F}(i)} \frac{A(f)}{A} Y_{6m}(\mathbf{r}_{ij}) \quad (1)$$

are calculated. Here, Y_{6m} are the spherical harmonics with $l = 6$, and the sum runs over all Voronoi neighbors. The connecting vector of the two neighboring particles i and j is \mathbf{r}_{ij} . The surface of the Voronoi cell A is defined by the sum over the corresponding facet areas $A(f)$ [$A = \sum_{f \in \mathcal{F}(i)} A(f)$]. Then, the complex vector is normalized over all possible orders m given by

$$\tilde{q}_{6m}(i) = \frac{q_{6m}(i)}{\sqrt{\sum_{m=-6}^6 |q_{6m}(i)|^2}}. \quad (2)$$

If, for neighboring particles i and j , the product

$$S_{ij} = \sum_{m=-6}^6 \tilde{q}_{6m}(i) \cdot \tilde{q}_{6m}^*(j) \quad (3)$$

is above 0.75, they are deemed to be connected (the asterisk $*$ stands for complex conjugation). With eight or more connections to its neighbors, a particle is defined to be in the solid state, and with less connections, to be in the liquid state [11].

Fractal objects are self-similar or scale invariant, which means, in a mathematical sense, that changing the scale produces similar structures. In contrast to the embedding Euclidean space, fractals have noninteger dimensions. One of the most commonly used procedures to determine the fractal dimension is the box-counting method [36]. Here, the minimum number of boxes $N(L)$ with the length L , which are needed to cover the fractal, are counted. The fractal dimension d_f is then given by [19]

$$d_f \propto \lim_{L \rightarrow 0} \frac{\log[N(L)]}{\log(1/L)}. \quad (4)$$

The probability for a specific particle to be in the solid state is called p . In percolation theory, the lowest probability for which the size of the largest cluster [37] reaches the same order as the size of the examined region is called the critical probability p_c . Following Ref. [23], the fractal dimension of a cluster with $p < p_c$ is zero. If p is clearly above p_c , the largest cluster is no longer fractal, so its dimension is given by the embedding Euclidean space. Only for $p = p_c$ (or slightly above) does the largest cluster have a fractal nature [23].

IV. RESULTS

Figure 1 shows the crystallization process of the complex plasma under gravity conditions. Directly after decreasing the rf power (at 0 s), hardly any particles are found in the solid state, indicating that due to the temporarily increased rf power, all particles obtain so much kinetic energy that no ordered structures can exist. After 244 s, most particles are in the solid state, confirming a timescale for crystallization of minutes. During the phase transition, the particles in the solid state create clusters. The clusters originate preferably from the lower part of the examined region. They grow mainly against the direction of gravity and are less pronounced in the horizontal direction. While the individual solid clusters increase in size, they merge with each other. Nevertheless, no compact crystallization front is observed.

Due to the crystallization process, the amount of particles in the solid state and therefore the probability p increases (see Fig. 1). The critical value for p is reached after about 178 s, when the largest solid cluster connects the upper with the lower boundary for the first time. The ratio of particles in the solid state and the total number of particles in the examined region give an upper limit of 0.3 for the critical probability p_c .

Figure 2 shows the amount $N(L)$ of boxes where at least one particle of the cluster is included versus the length of the boxes L in a double logarithmic scale. The slope of the linear fit gives a fractal dimension of $d_f = 2.72 \pm 0.03$. Changing the threshold for connected particles (3) varies the number of particles identified to be in the solid or liquid state. At a lower threshold the critical probability p_c is reached earlier, while at a higher threshold it is achieved later. Nevertheless, the absolute value for the fractal dimension at (or slightly above) the critical probability remains constant. Since the fractal dimension appears to be time independent, we do not expect that a finite scanning time affects its value. Of course, the exact structure of a cluster at a certain moment cannot be extracted. After all, this does not have an influence on the final results.

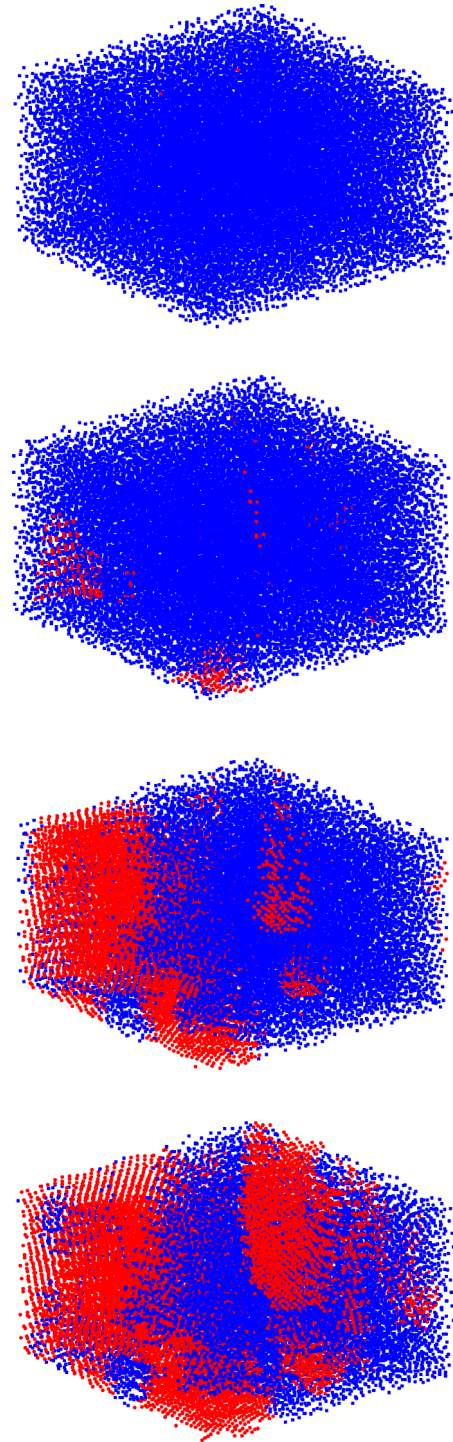


FIG. 1. The positions of particles in the solid (red/light) and liquid (blue/dark) state, 0, 66, 178, and 244 s (from top to bottom) after the crystallization process has begun. Due to their high thermal speed, the absolute position of the particles in the liquid state may have an error.

In Fig. 3 the distance to the nearest neighbor as well as the density of the particles are plotted, based on particles embedded completely in the solid state. Due to gravity, the interparticle distances are compressed. Averaged over all times in a cluster, the density of particles increases from $78 \pm 3 \text{ mm}^{-3}$

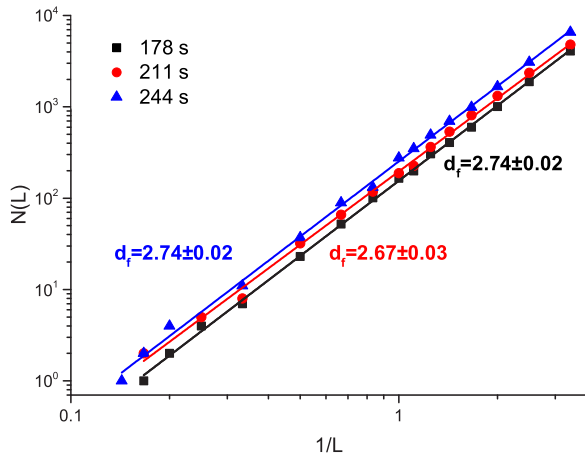


FIG. 2. The relation between the minimum amount of boxes needed to cover the largest solid cluster $N(L)$ and the corresponding length of the box L . The scans are done at 178 s, 211 s, and 244 s after the start of crystallization.

in the upper 20% to $87 \pm 3 \text{ mm}^{-3}$ in the lower 20% of the examined region. While crystallization progresses, the mean number density of particles and the average interparticle distance as well as their standard deviations remain constant over time. In previous experiments it was shown that the variation of particle density or interparticle distance during a phase transition was very small [8,13].

V. CONCLUSION

The crystallization process of a three-dimensional complex plasma with more than 36000 particles under gravity conditions was resolved temporally and spatially. To this end, at different times after the start of crystallization, a space-resolved local method was used to identify whether each single

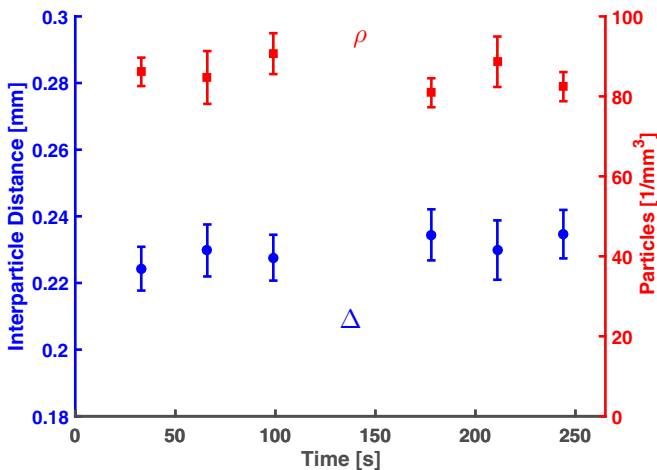


FIG. 3. The particle density (calculated by the inverse volume of the Voronoi cell [29]) and the distance to the nearest neighbor for particles within a cluster depending on the time after starting the crystallization. The standard deviation in each time step is given by the error bars.

particle was in the solid or liquid state. It has been confirmed that the timescales and size scales for phase transitions in a complex plasma are in a range of a few minutes and millimeters, respectively. The plasma parameters are in a steady state only microseconds after the rf power is lowered [38] and the charge of the particles needs milliseconds to be in equilibrium. During the crystallization process, no significant change of the particle density took place. The different timescales of the involved processes allowed the assumption that the background plasma and the mean charge of the particles were constant.

Crystallization takes place by the growth of different solid clusters, starting from the lower part under gravity. These clusters primarily expand vertically and, secondarily, horizontally. At later times they merge with each other. About 178 s after the start of crystallization, the extent of the largest solid cluster was in the range of the size of the examined region. At this time, the probability to determine a specific particle to be in the solid state was about 0.3, resulting in a critical value of $p_c \lesssim 0.3$. After the critical probability was attained, the box-counting method yielded a fractal dimension of $d_f = 2.72 \pm 0.03$, which lies between the values for epitaxial growth ($d = 3$) and for diffusion-limited growth ($d_f \approx 2.5$), indicating the observed crystallization process was governed by both growth mechanisms. This observation is in accordance with former observations of complex plasmas in two dimensions [13]. Since the calculated fractal dimension is much higher than for diffusion-limited cluster-cluster growth ($d_f \approx 1.8$), this phenomenon can be excluded as the dominant growth process. Since reversibility can also increase the fractal dimension, reversible diffusion-limited aggregation could also contribute to the observed fractal dimension of $d_f = 2.72 \pm 0.03$.

It should be kept in mind that, in contrast to the formal mathematical definition of a fractal in a physical system, self-affinity is only realized in a certain range, since it has a lowest size (at least one interparticle distance $\propto 0.2 \text{ mm}$) and a largest size (diameter of the examined region $\propto 10 \text{ mm}$). Due to this limitation, the method which is utilized to determine the fractal dimension could influence the result [36,39]. Furthermore, it could not be excluded, based on the limited time resolution, that the critical value for the probability was reached before the scan was done. This could have an effect on the calculated fractal dimension, if the measured probability was significantly larger than the critical value. Nevertheless, Fig. 2 shows no strong time dependence for the fractal dimension. Besides this, no measurable changes in number density or in interparticle distances were observed within the clusters during crystallization.

All observed effects are in good agreement with former experiments, using two-dimensional data. Due to their lower damping rate compared to colloidal systems, complex plasmas are a valuable tool for understanding phase transitions in three dimensions.

ACKNOWLEDGMENTS

This work was supported by DLR under Grant No. 50 WM1442. The authors want to thank Julian Kaupe for helpful discussions.

- [1] J. Anwar and D. Zahn, *Angew. Chem., Int. Ed.* **50**, 1996 (2011).
- [2] T. Palberg, *J. Phys.: Condens. Matter* **11**, R323(R) (1999).
- [3] V. E. Fortov, A. V. Ivlev, S. A. Khrapak, A. G. Khrapak, and G. E. Morfill, *Phys. Rep.* **421**, 1 (2005).
- [4] A. P. Nefedov, G. E. Morfill, V. E. Fortov, H. M. Thomas, H. Rothermel, T. Hagl, A. V. Ivlev, M. Zuzic, B. A. Klumov, A. M. Lipaev, I. V. Molotkov, O. F. Petrov, Y. P. Gidzenko, S. K. Krikalev, W. Shepard, A. I. Ivanov, M. Roth, H. Binnenbruck, J. A. Goree, and Y. Semenov, *New J. Phys.* **5**, 33 (2003).
- [5] T. Palberg, *Curr. Opin. Colloid Interface Sci.* **2**, 607 (1997).
- [6] E. B. Tomme, D. A. Law, B. M. Annaratone, and J. E. Allen, *Phys. Rev. Lett.* **85**, 2518 (2000).
- [7] H. M. Thomas and G. E. Morfill, *Nature (London)* **379**, 806 (1996).
- [8] T. Sheridan, *Phys. Plasmas* **15**, 103702 (2008).
- [9] A. Melzer, A. Homann, and A. Piel, *Phys. Rev. E* **53**, 2757 (1996).
- [10] C. A. Knapik, D. Samsonov, S. Zhdanov, U. Konopka, and G. E. Morfill, *Phys. Rev. Lett.* **98**, 015004 (2007).
- [11] B. Steinmüller, C. Dietz, M. Kretschmer, and M. Thoma, *Phys. Plasmas* **24**, 033705 (2017).
- [12] M. Zuzic, A. V. Ivlev, J. Goree, G. E. Morfill, H. M. Thomas, H. Rothermel, U. Konopka, R. Sütterlin, and D. D. Goldbeck, *Phys. Rev. Lett.* **85**, 4064 (2000).
- [13] M. Rubin-Zuzic, G. Morfill, A. Ivlev, R. Pompl, B. Klumov, W. Bunk, H. Thomas, H. Rothermel, O. Havnes, and A. Fouquet, *Nat. Phys.* **2**, 181 (2006).
- [14] B. A. Klumov and G. Morfill, *JETP Lett.* **90**, 444 (2009).
- [15] T. Terao and T. Nakayama, *Phys. Rev. E* **58**, 3490 (1998).
- [16] P. Dimon, S. K. Sinha, D. A. Weitz, C. R. Safinya, G. S. Smith, W. A. Varady, and H. M. Lindsay, *Phys. Rev. Lett.* **57**, 595 (1986).
- [17] S. D. Orrite, S. Stoll, and P. Schurtenberger, *Soft Matter* **1**, 364 (2005).
- [18] A. C. Levi and M. Kotrla, *J. Phys.: Condens. Matter* **9**, 299 (1997).
- [19] T. Vicsek, *Fractal Growth Phenomena*, 2nd ed. (World Scientific, Singapore, 1992).
- [20] T. A. Witten, Jr., and L. M. Sander, *Phys. Rev. Lett.* **47**, 1400 (1981).
- [21] In the DLCA model, particles are distributed randomly. In each “time step,” an arbitrary chosen particle or cluster is moved in any direction. If a particle or a cluster touches another particle, they stick together.
- [22] Following the DLA model, one after another particle starts far from a single cluster and walks at random, until it arrives at the cluster and sticks to it.
- [23] A. Aharony and D. Stauffer, *Introduction to Percolation Theory*, 2nd ed. (Taylor & Francis, London, 2003).
- [24] S. A. Khrapak, A. V. Ivlev, and G. E. Morfill, *Phys. Rev. E* **70**, 056405 (2004).
- [25] A higher scanning velocity of ≈ 1.6 mm/s shows compatible results.
- [26] H. Thomas, G. Morfill, and V. Tsytovich, *Plasma Phys. Rep.* **29**, 895 (2003).
- [27] M. Thoma, M. Kretschmer, H. Rothermel, H. Thomas, and G. Morfill, *Am. J. Phys.* **73**, 420 (2005).
- [28] S. A. Khrapak, B. A. Klumov, P. Huber, V. I. Molotkov, A. M. Lipaev, V. N. Naumkin, A. V. Ivlev, H. M. Thomas, M. Schwabe, G. E. Morfill, O. F. Petrov, V. E. Fortov, Y. Malentschenko, and S. Volkov, *Phys. Rev. E* **85**, 066407 (2012).
- [29] V. N. Naumkin, D. I. Zhukhovitskii, V. I. Molotkov, A. M. Lipaev, V. E. Fortov, H. M. Thomas, P. Huber, and G. E. Morfill, *Phys. Rev. E* **94**, 033204 (2016).
- [30] J. C. Crocker and D. G. Grier, *J. Colloid Interface Sci.* **179**, 298 (1996).
- [31] Y. Ivanov and A. Melzer, *Phys. Plasmas* **12**, 072110 (2005).
- [32] A. Piel, *Plasma Physics: An Introduction to Laboratory, Space, and Fusion Plasmas* (Springer, Berlin, 2017).
- [33] W. Mickel, S. C. Kapfer, G. E. Schröder-Turk, and K. Mecke, *J. Chem. Phys.* **138**, 044501 (2013).
- [34] C. Dietz, T. Kretz, and M. H. Thoma, *Phys. Rev. E* **96**, 011301(R) (2017).
- [35] C. Dietz and M. H. Thoma, *Phys. Rev. E* **94**, 033207 (2016).
- [36] S. Buczkowski, S. Kyriacos, F. Nekka, and L. Cartilier, *Pattern Recognit.* **31**, 411 (1998).
- [37] A solid cluster is created by a group of particles in the solid state, which are Voronoi neighbors. This means such a cluster consists only of particles in the solid state, linked to each other by a chain of neighbors, also part of the cluster [23].
- [38] E. Carbone, N. Sadeghi, E. Vos, S. Hübner, E. Van Veldhuizen, J. Van Dijk, S. Nijdam, and G. Kroesen, *Plasma Sources Sci. Technol.* **24**, 015015 (2014).
- [39] B. B. Mandelbrot, *Phys. Scr.* **32**, 257 (1985).